Development of a Multispectral Texture Measurement Facility for Use in an EU Funded Study of the Naturalness of Surfaces

Montgomery Ruth[1], Pointer Michael[1], Goodman Teresa[1], Harvey Andy[2]

[1]*National Physical Laboratory, Hampton Road, Teddington, TW11 0LW, UK.*
[2]*School of Engineering and Physical Sciences, Heriot -Watt University.*

Abstract

The measurement of the appearance of a textured surface requires the precise evaluation of a number of physical attributes, such as gloss, reflectance and translucency, within a multi-angled goniometric system. Robust characterisation of the illumination, optical and geometric set-up and of the detector characteristics is required to ensure the results are validated and have a rigorous metrological basis.

The system described incorporates a multi-spectral imaging system, conceptually related to a Lyot filter, with 28 discrete spectral bands in the range from 370 nm to 800 nm. This facilitates characterisation of the target surface in both a spectral and spatial sense. The development of a series of algorithms tailored to the class of sample studied, e.g. wood, stone, fabric etc., coupled to a consistent taxonomy will allow an accurate description of natural and non-natural surfaces. The theoretical modelling and tolerances of this spectrometer are presented, together with experimental results demonstrating excellent agreement between the modelled spectral band profiles and those actually achieved.

The characterisation of surface textures will provide input to an EU-funded study measuring 'naturalness'. The 'Measurement of Naturalness' or 'MONAT' project will use the latest technology and scientific understanding in areas of metrology, instrumentation, cognitive neuroscience, psychology and mathematical modelling to give a cross-sector approach to understanding the relevant perceptual processes. The results of an outline study into the perception of naturalness for samples of natural and synthetic wood is discussed briefly in Section 4 and more comprehensively in [1].

Keywords: Lyot, spectral, goniometric, appearance, naturalness

1. Introduction

1.1 Applications of multispectral texture measurements

Multispectral analysis of textured surfaces is important in many sectors, including earth observation, recycling, paper manufacturing, mineralogy, medicine, biology, cosmetic and other personal health-care industries. As an example, appearance is one of the most critical parameters affecting consumer choice in the retail food industry. Food processors are eager to develop systems that can accurately assess the quality or freshness of their products, and thereby discard those products that fall short of their quality control standards. Currently this job is done manually by factory workers and is usually a totally subjective process. Accurate appearance measurement scales that combine textural and spectral information would be a valuable aid in the assessment of the freshness of fruit, vegetables and meat [2], the texture of food surfaces, and the

non-uniformity in the colouration of confectionary products (which is often a result of oxidation).

In medical imaging, images recorded in a variety of spectral bands can give information about the amount of oxygen in the blood and about blood perfusion in various parts of the body, including the extremities or organs such as the eyes [3]. This can be important when monitoring the health of patients with conditions such as heart disease, diabetes or blue-baby syndrome. Furthermore, in the field of ophthalmology, an ability to measure haemoglobin oxygenation using retinal images provides useful information for the diagnosis of conditions such as diabetic retinopathy, age-related macular degeneration and glaucoma.

1.2 The EC MONAT project

The EU MONAT project is part funded under the 'Measuring the Impossible' Theme of the Framework 6 New and Emerging Science and Technology (NEST) Programme. The project focuses on the measurement of the perceived naturalness of surfaces: a property of a material that is reasonably easy to define and that has minimal cultural or gender bias. A key aspect of the study will be to develop a basic understanding of how the human visual system (HVS) perceives and categorises natural or non-natural surfaces. Many 'data reduction' processes are performed within the HVS in order to make the transition from the physical response (nerve impulses generated when light from the object falls on the retina) to the final visual perception and categorisation in the brain. The HVS also copes transparently with factors such as changes in the illumination, which alter the reflectance, colour and gloss, thus changing the appearance of the surface. The development of automated instrumentation that is able to interpret a scene not just in terms of its physical characteristics, but also in terms of how it would be perceived and categorised by a human observer, is thus a complex and challenging task. The MONAT project aims to address some of these issues by seeking to identify some of the sensory and cognitive processes associated with the perception of naturalness and by developing and using leading edge measurement equipment to perform accurate physical measurements of the materials being studied.

1.3 Spectral measurements

Analysing surfaces and objects in terms of their spectral characteristics, using a spectrometer, reveals information that would be otherwise inaccessible via the broadband response functions of the human visual system. This has led to huge advances in many areas of science and technology, such as remote sensing, astronomy, medicine, production and manufacturing [4-10].

Spectrometers use various methods to acquire spatial and spectral information including: whiskbroom (zero-dimensional); pushbroom-scanning (one-dimensional with FOV movement) [11-13]; staring (two-dimensional with stationary FOV) [14]; and windowing (two-dimensional with FOV movement) [15]. Staring instruments are most common and employ a two–dimensional FOV, which remains fixed on the

object; the scene and image do not move with respect to one another. Spectral discrimination is performed using tuneable filters or imaging interferometers, including filter wheels, acousto-optic techniques, LCTF, IRIS, BIREFTIS or foveal systems, [14, 16, 17, 18]. The advantages (Fellget, Jacquinot) and disadvantages of Fourier Transform (FT) devices are discussed in [19].

Information on the spectral variation across a non-uniform surface can be obtained using many of these approaches, by either spatial or spectral multiplexing of time sequential images, although this limits the application to situations in which the data can be reconstructed faster than the scene varies. To avoid this problem, the system being developed at NPL uses a 'snapshot' approach, in which spatial and spectral information is obtained simultaneously (see Section 2). This has the advantage that no temporal mis-registration is introduced between capture of the spatial and spectral information. The disadvantage is that there is the trade-off between the number of simultaneously viewed spectral images and the spatial resolution of those images.

2. Instrument Theory

2.1 The LYOT filter

The multi-spectral texture measurement system being developed for the MONAT project is based on a Lyot filter [9]. This was originally developed to enable movements of the solar atmosphere to be observed and to allow photography of the corona of the sun at times other than during a solar eclipse. It permits simultaneous observation of different points of an extended luminous source in narrow spectral regions, with minimal loss of light. The original device operated from 380 nm to 2000 nm, with an optimum resolution of 0.1nm for green light.

The Lyot filter is composed of multiple waveplates sandwiched between co-aligned linear polarisers, which are aligned to pass light polarised at 45 ° to the fast axis of each waveplate. The waveplates are cut parallel to the optic axis and are made from birefringent material, which introduces a phase delay between the orthogonally polarised components.

The relative phase difference introduced between the *x* and *y* components of the wave energy, after traversing a waveplate of thickness d_1, is given by:

$$\Delta\phi = \frac{2\pi d_1}{\lambda_o}(n_o - n_e) \qquad (1)$$

where λ_0 is the primary wavelength, and n_o and n_e are the refractive indices of the ordinary and extraordinary waves. (n_o-n_e) is referred to as the birefringence. Thus each of the polariser-waveplate pairs results in a high intensity central maxima, with low intensity side lobes. The transmission function for each polariser-waveplate pair is proportional to:

$$\cos^2[d_1\pi\left(\frac{n_e - n_o}{\lambda}\right)].$$

In the Lyot filter, each of the successive waveplates has a thickness which is double that of the preceding one. As the number of waveplate-polariser pairs increases, so the separation between the central maxima also increases. The system can be designed such that only one bright maximum is formed when the system is used with a defined, limited, input spectrum. Fig. 1 demonstrates the reduction in the FWHM and the increase in the number of side lobes as the waveplate-polariser pairs is increased from one to three.

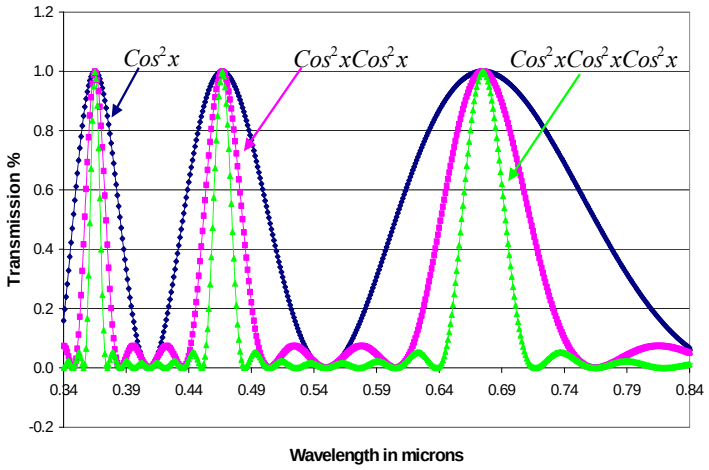

Fig. 1. Demonstration of polariser retarder pairs in a Lyot filter; increase in number of pairs reduces FWHM of cyclic maxima.

2.2 The IRIS system of Harvey and Fletcher-Holmes

Harvey and Fletcher-Holmes [14] further developed the Lyot filter to produce an Image Replication Imaging Spectrometer or IRIS system (Fig. 2). They replaced the polarisers of the Lyot filter with Wollaston polarising beam splitters, which introduce a spatial separation of the input image, creating pairs of replicated images (in all other respects, the theory and physical mechanism of the spectral discrimination remain unchanged).

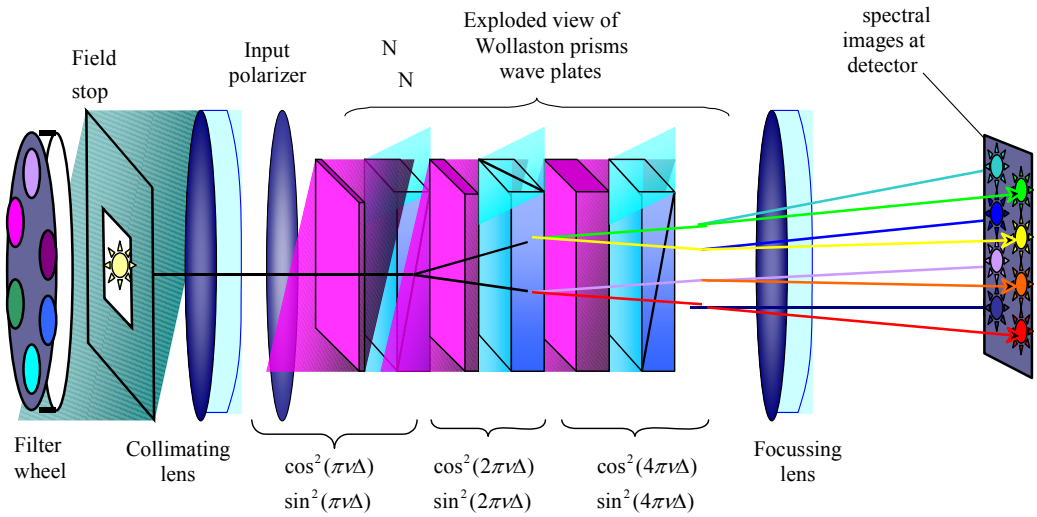

Fig. 2. Image Replication Imaging Spectrometer (IRI S) with filter wheel addition.

Harvey and Fletcher-Holmes also deviated from the two times thickness ratio described by Lyot. This results in a breakdown in the cyclic nature of the system, but since they only required eight spectral bands, within a region prescribed by their passsband filters, neighbouring maxima were irrelevant. Instead they wished to orthogonalise these eight peak bands, additionally maximising the maxima and minimising the side lobes.

2.3 The NPL system

The system being developed at NPL uses Wollaston polarising beam splitters but, unlike the Harvey and Fletcher-Holmes system, in this case the two times thickness ratio of the waveplates has been re-instated. The system uses three waveplate-prism pairs, generating transmittance profiles with the general form:

$$T_1 = \cos^2[d_1\pi\left(\frac{n_e - n_o}{\lambda}\right)]\cos^2[d_2\pi\left(\frac{n_e - n_o}{\lambda}\right)]\cos^2[d_3\pi\left(\frac{n_e - n_o}{\lambda}\right)] \qquad (2)$$

Thus a series of cyclically-repeating transmittance profiles is generated, as described in the original Lyot paper (note the ‘folded over’ rather than ‘sequentially repeated’ characteristic – see Fig. 3) but, unlike Lyot, each of these is spatially separated to form eight distinct images. Thus, for example, the transmittance curve represented by the blue line in Fig. 3 forms a separate image to that represented by the yellow line, and so on. Each of the images contains several transmittance peaks but, by introducing cut-on and cut-off filters, the NPL system allows blocks of eight peaks (one in each image) to be isolated sequentially.

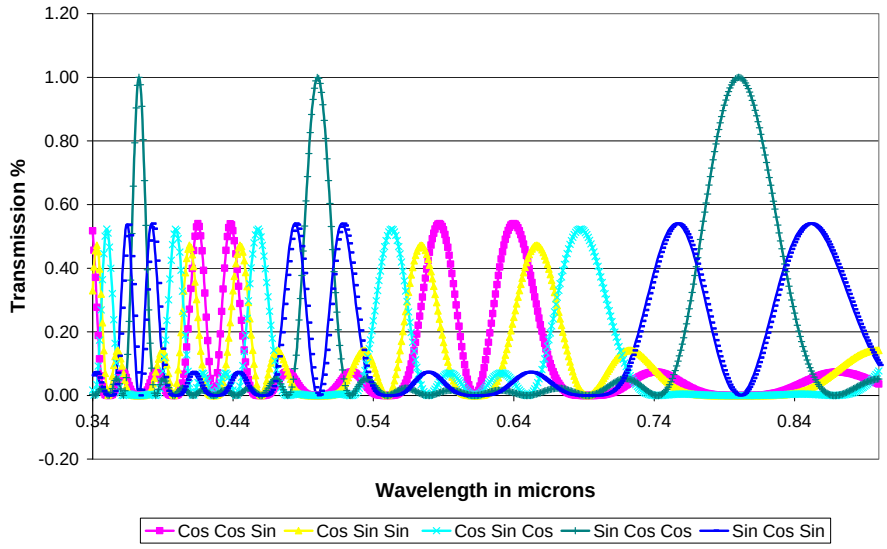

Fig. 3. Spectral transmission profiles of the NPL system using Quartz waveplates of thickness 135, 270 and 540 microns.

The waveplate thicknesses in the NPL system have been chosen such that four sets of transmittance maxima fall within the visible region of the spectrum. A double filter wheel with specifically selected cut-on and cut-off filters is used to isolate, in sequence, one of four contiguous spectral bands, each containing eight bell-shaped maxima (one from each waveplate-polariser pair) - see Fig. 4. The system is designed such that each successive region contains one peak from the previous one, to allow normalisation between the regions.

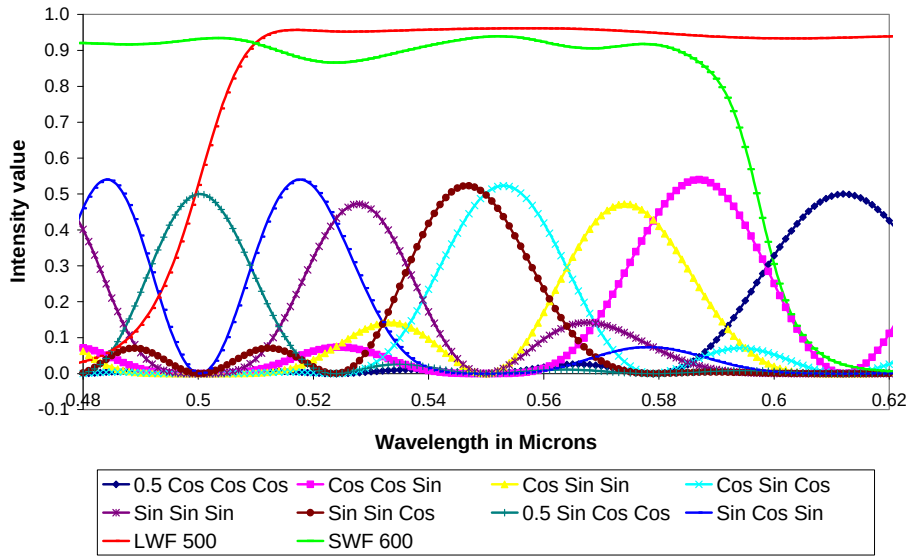

Fig. 4. Transmission profiles of long and short wave pass filters overlaid on IRIS spectral transmission profiles in the range 480-620 nm.

2.4 Illumination and filtering

The illumination source is a tungsten halogen lamp. This has a spectrum that is a close approximation to a Planckian Black body radiator, with a colour temperature of approximately 3100 K. It is of a type frequently used as a transfer standard for spectral irradiance measurements [20].

Spectral filters used for metrological applications should ideally be:

- Spatially uniform
- Spectrally smoothly varying bandpass
- Stable with time
- Insensitive to temperature
- Insensitive to angle of incidence
- Fully opaque to wavelengths outside of desired band pass

In designing our filter system we have tried to optimise based on the above.

In order that a single image contains only one transmittance peak at any one time, a series of calibrated cut-on/long-wave pass and cut-off /short-wave pass filters are placed, in pairs, between the light source and the prisms. The chosen filters have a hard dielectric coating and interference effects rather than absorption to isolate the spectral bands. Any misalignment of the filters with respect to the normal to the incident radiation will lead to a shift to shorter wavelengths; this is allowed for as part of the calibration uncertainty budget.

2.5 Modelling of the waveplates

The system has been designed such that twenty-eight transmittance maxima are contained within the spectral range from 370 nm to 800 nm. Many birefringent materials are capable of achieving this, but the additional factors of availability, cost, manufacturing tolerances and manipulation also needed to be considered as part of the design. The spectral transmission profiles were therefore calculated for a range of materials, using equation 3, to allow the optimum solution to be found. The modelling involved varying the thicknesses of each of the three waveplates for each material, but maintaining the two-times thickness ratio throughout.

$$T_1 = \cos^2[d_1\pi\left(\frac{n_e - n_o}{\lambda}\right)]\cos^2[d_2\pi\left(\frac{n_e - n_o}{\lambda}\right)]\cos^2[d_3\pi\left(\frac{n_e - n_o}{\lambda}\right)]$$

$$T_2 = \cos^2[d_1\pi\left(\frac{n_e - n_o}{\lambda}\right)]\cos^2[d_2\pi\left(\frac{n_e - n_o}{\lambda}\right)]\sin^2[d_3\pi\left(\frac{n_e - n_o}{\lambda}\right)]$$

$$T_3 = \cos^2[d_1\pi\left(\frac{n_e - n_o}{\lambda}\right)]\sin^2[d_2\pi\left(\frac{n_e - n_o}{\lambda}\right)]\cos^2[d_3\pi\left(\frac{n_e - n_o}{\lambda}\right)]$$

etc ……. (3)

The most up-to-date coefficient values were used; for Calcite and Quartz this was from G. Ghosh, using Sellmeier equation 4 [21]. Calcite was discounted because the 4.95, 9.9 and 19.8-micron thickness required for the plates would have proved extremely difficult to manipulate (it would have been possible to cement the waveplates onto optical blanks to increase their thickness, but this was not the preferred option since it was desirable to minimise the number components that would be integrated into the final system). MgF and $SrMoO_4$ were rejected due to lack of availability. Finally 135, 270, 540 micron waveplates using quartz were chosen, without the use of any substrate.

By altering the waveplate thicknesses from 135, 270 and 540 microns, adding and subtracting 1 or 2 microns in either direction, tolerance graphs were plotted, as in Fig. 5. Introducing such a deviation from the strict two-times ratio clearly leads to a loss in the inherent symmetry of the graphs. Several of the maxima lose energy, which is redistributed to the side lobes, thereby reducing the dynamic range of the system. A tolerance of ±0.5 microns was therefore set on the waveplate thickness. The flatness of the waveplates was specified in terms of the wavefront distortion (λ/8 peak to valley at 632.8 nm) and the parallelism was specified as 3 arc seconds, which equates to a tolerance in the flatness of 0.291 microns for the 20 mm square waveplates used, or λ/2 at 600 nm.

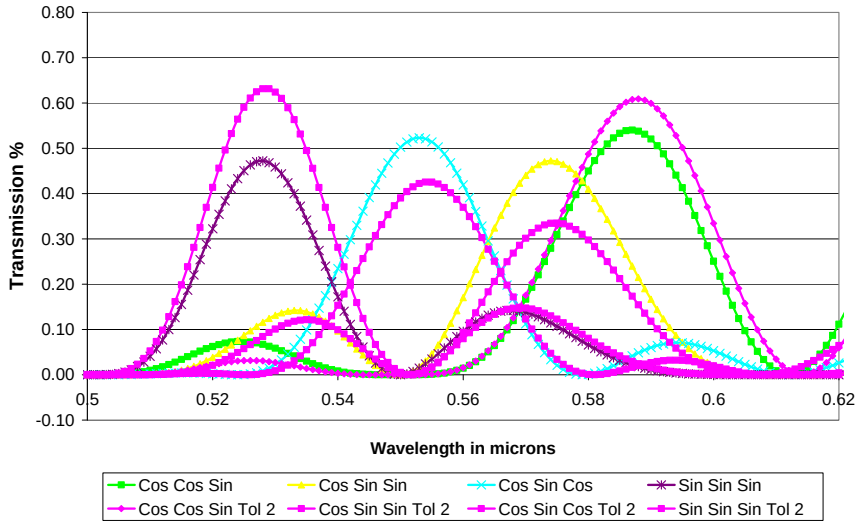

Fig. 5. Effect of introducing a deviation in the waveplates from a strict two-times thickness ratio. Two-micron tolerances are shown.

2.6 Zemax modelling of the prisms

The required dimensions for the prisms (thickness and angular cut) were modelled using Zemax-EE optical design software. A separate configuration, based on tracing an ordinary or extra-ordinary ray through the prisms, and use of Jones matrices [22], was required for each of the transmission functions. Fig. 6 shows all eight configurations, each highlighted with a different colour. Although prisms are typically used as dispersive devices, the chromatic aberration of the images in this case was kept to acceptable levels because (a) only a small range of wavelengths contained in

the spectral peak is transferred along any one path and (b) the system uses prism-prism pairs, which goes some way to cancelling the dispersion. Inter-reflections between the quartz and calcite sandwiched optics can significantly affect the quality of the final images. Various methods are being considered in order to minimise these effects, including the use of index-matching fluid and cementing the optics together.

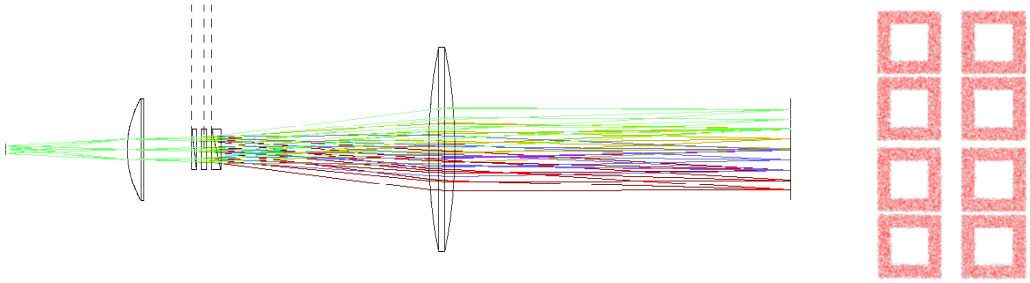

Fig. 6. Zemax modelling of IRIS device (left) and predicted spatial distribution at the image plane (right).

The calculation of the prism angles was performed such that the space-bandwidth product was optimised i.e. to optimise the trade-off between the number of simultaneously viewed spectral images and the resolution of those images. When an increased image resolution is required and a reduction in the number of spectral bands can be tolerated, then the system can be configured to isolate just four of the eight images.

2.7 The Camera

The camera chosen for use in the system is a SPOT, Insight Firewire 4 Megapixel monochrome device, designed for use in machine vision, metrology and other industrial applications. This has a 4-megapixel CCD with a 15.1x15.1 mm^2 area, which allows a wide field of view, coupled to high resolution. The 14 bit-depth in real time capture mode is at the upper end of the required specification and allows image enhancement.

3. Theory Versus Practical Results

An Ocean Optics S1000 fibre optic spectrometer was used to carry out preliminary verification tests of the spectral transmission of the NPL IRIS system. A fibre-optic light-pipe coupled to a diffuser was imaged through the polariser, prisms and waveplates, forming an image in free space. The fibre-optic coupled to the spectrometer was suspended in the image plane and the spectral content of the light forming each of the eight images was recorded. The measurements were repeated at several spatially separated points across each image. The results were normalised against the source radiance and all values were dark corrected. Fig. 7 shows two graphs showing the theoretical and measured individual transmission spectra.

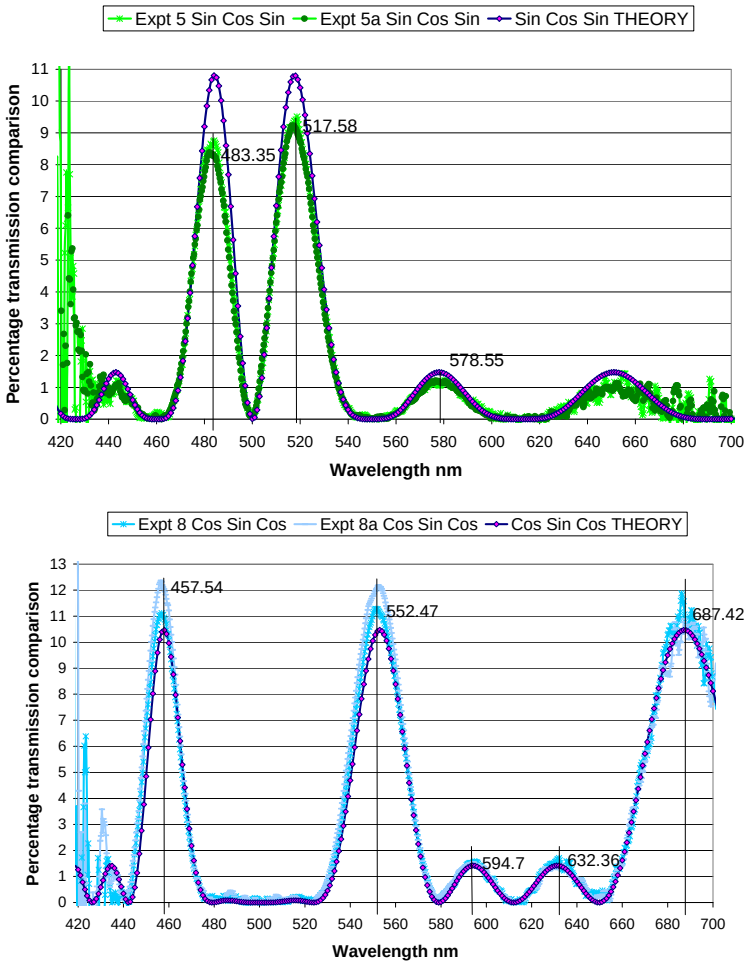

Fig. 7. Agreement between theory and practical results for spectral transmission profiles.

Although these results have not been wavelength corrected and cannot be considered a calibrated measurement, their fidelity with the theoretical profiles is very encouraging. Any drift of wavelength position or loss of dynamic range due to increased energy in the side lobes at the expense of the central maxima, as a result of sensitivity to deviation from the two-times thickness ratio, lack of parallelism, or out of tolerance thickness, has been avoided. It appears, therefore, that the manufacturing of the optics has been well within specified tolerances.

As the next stage in the development of a system for texture measurements, this IRIS device will be placed on the NPL's Gonio Apparent Spectro Photometer (GASP) stage, to allow full goniometric spatial and spectral characterisation of surfaces.

4. Naturalness Experiments

The results of a preliminary study in preparation for the EU MONAT project ('MONAT Zero') are presented in [1]. The paper describes the visual and touch assessment of twenty-two wood and wood-effect samples from a variety of different manufacturers. The samples were mounted in identical sealed containers with a grey

surround and an 8x8 cm^2 viewing window. Thirty-eight observers completed a series of four timed experiments to place randomised samples in each of five categories:

Definitely natural
Probably natural
Undecided
Probably not natural
Definitely not natural

A weighted scale was then used to assess each participant's degree of success in correctly categorising the samples. The results were analysed to identify any bias based on time of day of experiment, age, gender, scientific background, educational achievement etc. No such biases were observed, although the authors would like to emphasise that the data set was rather small. The full MONAT study will involve a much larger number of observers and a much wider range of experimental investigations.

Other experimental observations from the MONAT Zero study included:

- It is important to impose a time restriction: observers should be allocated enough time to make a judgement based on a first impression, but not so long that an emotional response of preference is introduced.
- It is essential to present all the samples to the observers in the same way and to remove any additional cues, such as being able to see the edges or backing of the samples or feel differences in their weights.
- The understanding of the term 'naturalness' varied between the observers. This highlights the importance of providing a clear taxonomy for the EU MONAT project.
- Observers stated that the key visual factors influencing their decisions were grain texture and pattern regularity. Several identified 'randomness' as an important property of natural materials. The physical measurement and modelling of these parameters will therefore form a strong element of the EU MONAT project.

References

1. R. Montgomery, T. Goodman, M. Pointer and A. Harvey. "The measurement of multispectral texture and its contribution to an EU funded study of the naturalness of surfaces". *CIE Appearance Symposium 2006*, Paris. (In press).
2. S. Kong, Y. Chen, I. Kim and M. Kim. "Analysis of hyperspectral fluorescence images for poultry skin tumour inspection". *Applied optics,* ***43,*** No4, 2004
3. S. Ramachandran, N. Taylor, A. McNaught and A Harvey. "Modelling of light propagation in retinal tissue". *SPIE,* **Vol. 5486**, p 48-60, July 2004
4. D. Torr, M. Zukic, C. Feng, A. Ahmed, W. Swift. "Miniaturised high-resolution NUV-VIS-NIR imaging spectrometer array for FAST SAT applications". *Proc. of SPIE*, Vol. 2266, p206-220, 1994
5. M. Descour, C. Volin, E. Dereniak, K. Thome, A. Schumaker, D. Wilson and P. Maker. "Demonstration of a high speed non-scanning imaging spectrometer". *Optics Letters*, **Vol. 22**, No.16, 1997
6. J. Graham. "IFIRS: An Imaging Fourier transform spectrometer for the next generation space telescope". *ArXiv:astro-ph/9910442v1*, 1999

7. D. Naylor, B. Gom, I. Schofield, G. Tompkins and G. Davis. Mach-Zender "Fourier transform spectrometer for astronomical spectroscopy at submillimeter wavelengths". *Proc. of SPIE,* **Vol. 4855**, pp. 540-551, 2003
8. F. Grandmont, L. Drissen, G. Joncas. "Development of an imaging Fourier transform spectrometer for astronomy". *Proc. of SPIE,* 2002
9. B. Lyot. "Un Monochromateur EO champ utilisant les interference en lumiere polarisee". *Compt Rend. Hebd. Seanc. Acad. Sci.,* **Vol. 197**, p1593-1595
10. J. Leroy. "Solc elements in Lyot-Ohman filters". *J. optics,* **Vol.1**, No.5. pp293-304, 1980
11. P. Mouroulis, J. Shea and D. Thomas. "Design, tolerancing and alignment for pushbroom imaging spectrometers for high response uniformity". *Proc. SPIE,* **Vol. 4441**, pp106-117, 2001
12. Compact High Resolution Imaging Spectrometer. (CHRIS). Developed by Sira and ESA. www.chris-proba.org.uk
13. Airborne Visible/Infrared Imaging Spectrometer (AVIRIS). http://aviris.jpl.nasa.gov/
14. A. Harvey and D. Fletcher -Holmes. "High throughput snapshot spectral imaging in two dimensions". *Proc of SPIE,* **Vol. 4959**, pp46-54, 2003
15. R. Sellar, G. Boreman, L. Kirkland. "Comparison of signal collection abilities of different classes of imaging spectrometers". *Proceedings of SPIE*, **Vol. 4816**, pp.389-396, 2002
16. D. Fletcher -Holmes and A. Harvey. "Real time imaging with a hyperspectral fovea". *J.Opt, A. Pure Appl. Opt*., **7**, S298-S302, 2005
17. A. Harvey and D. Fletcher–Holmes. "Birefringent Fourier transform imaging spectrometer". *Optics Express* **Vol. 12**, No.22, 2004
18. www.cri-inc.com/products/maestro.asp
19. R. Sellar, G. Boreman, L. Kirkland. Comparison of signal collection abilities of different classes of imaging spectrometers. Proceedings of the SPIE, Vol. 4816, pp. 389-396. (2002).
20. E.R. Woolliams, N.P.Fox, M.G. Cox, P.M. Harris, N.J. Harrison, "Final report on CCPR K1-a: Spectral irradiance from 250 nm to 2500 nm". *Metrologia,* **43**, Tech. Suppl., 02003, 2006. http://kcdb.bipm.org/AppendixB/default.asp
21. Ghosh, "Dispersion-equation coefficients for the refractive index and birefringence of calcite and quartz crystals". *Optics Communications*, **Vol. 163**, pp. 95-102, 1999
22. Zemax optical design program user's guide. Version 10.0. www.focus-software.com

Acknowledgements

The authors would like to thank Julie Taylor, Nigel Fox, Neil Harrison and Eric Usadi of NPL for useful discussions relating to the development of the IRIS system.

This work was supported by the National Measurement System Policy Unit of the Department of Trade and Industry.